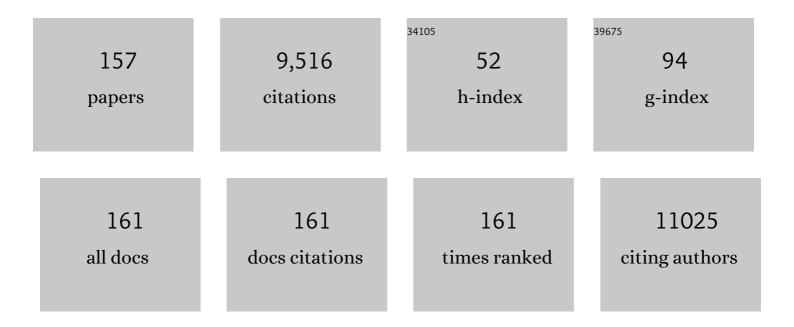
Angus I Kirkland

List of Publications by Year in descending order

Source: https://exaly.com/author-pdf/1470026/publications.pdf Version: 2024-02-01



#	Article	IF	CITATIONS
1	Trainable segmentation for transmission electron microscope images of inorganic nanoparticles. Journal of Microscopy, 2022, 288, 169-184.	1.8	7
2	Contrast transfer and noise considerations in focused-probe electron ptychography. Ultramicroscopy, 2021, 221, 113189.	1.9	28
3	Platinum supported on pristine and nitrogen-doped bowl-like broken hollow carbon spheres as oxygen reduction reaction catalysts. Journal of Applied Electrochemistry, 2021, 51, 991-1008.	2.9	9
4	Oleylamine Aging of PtNi Nanoparticles Giving Enhanced Functionality for the Oxygen Reduction Reaction. Nano Letters, 2021, 21, 3989-3996.	9.1	37
5	Ptychographic Single Particle Analysis for Biological Science. Microscopy and Microanalysis, 2021, 27, 190-192.	0.4	1
6	Quantifying the performance of a hybrid pixel detector with GaAs:Cr sensor for transmission electron microscopy. Ultramicroscopy, 2021, 227, 113298.	1.9	12
7	Elmar Zeitler (1927–2020). Ultramicroscopy, 2021, 229, 113366.	1.9	0
8	Parakeet: a digital twin software pipeline to assess the impact of experimental parameters on tomographic reconstructions for cryo-electron tomography. Open Biology, 2021, 11, 210160.	3.6	5
9	A fundamental look at electrocatalytic sulfur reduction reaction. Nature Catalysis, 2020, 3, 762-770.	34.4	455
10	Transforming carbon dioxide into jet fuel using an organic combustion-synthesized Fe-Mn-K catalyst. Nature Communications, 2020, 11, 6395.	12.8	161
11	Low Dose Electron Ptychography for Cryo-biological Imaging. Microscopy and Microanalysis, 2020, 26, 1488-1490.	0.4	0
12	Detectors—The ongoing revolution in scanning transmission electron microscopy and why this important to material characterization. APL Materials, 2020, 8, .	5.1	44
13	Low-dose phase retrieval of biological specimens using cryo-electron ptychography. Nature Communications, 2020, 11, 2773.	12.8	72
14	A 3D map of atoms in 2D materials. Nature Materials, 2020, 19, 827-828.	27.5	0
15	Phase reconstruction using fast binary 4D STEM data. Applied Physics Letters, 2020, 116, .	3.3	34
16	STEM and Elemental Analysis by EDS and EELS for Two-dimensional Atomic Structure Containing Au and Cu. Microscopy and Microanalysis, 2019, 25, 1776-1777.	0.4	0
17	Three-Dimensional Imaging of Nanoparticle Chemistry Using Spectroscopic Single Particle Reconstruction. Microscopy and Microanalysis, 2019, 25, 400-401.	0.4	0
18	Simultaneous Identification of Low and High Atomic Number Atoms in Monolayer 2D Materials Using 4D Scanning Transmission Electron Microscopy. Nano Letters, 2019, 19, 6482-6491.	9.1	36

#	Article	IF	CITATIONS
19	Electron ptychography using an ultrafast direct electron detector. Microscopy and Microanalysis, 2019, 25, 20-21.	0.4	1
20	Contrast Transfer and Noise Minimization in Electron Ptychography. Microscopy and Microanalysis, 2019, 25, 64-65.	0.4	3
21	Three-dimensional Electron Ptychography of Catalyst Nanoparticles using Combined HAADF STEM and Atom Counting. Microscopy and Microanalysis, 2019, 25, 8-9.	0.4	3
22	Observing Structural Dynamics and Measuring Chemical Kinetics in Low Dimensional Materials Using High Speed Imaging. Microscopy and Microanalysis, 2019, 25, 1682-1683.	0.4	2
23	Low-Dose Scanning Electron Diffraction Microscopy of Mechanochemically Nanostructured Pharmaceuticals. Microscopy and Microanalysis, 2019, 25, 1746-1747.	0.4	6
24	3D Electron Ptychography. Microscopy and Microanalysis, 2019, 25, 1802-1803.	0.4	2
25	Imaging Three-Dimensional Elemental Inhomogeneity in Pt–Ni Nanoparticles Using Spectroscopic Single Particle Reconstruction. Nano Letters, 2019, 19, 732-738.	9.1	18
26	Atomic electrostatic maps of 1D channels in 2D semiconductors using 4D scanning transmission electron microscopy. Nature Communications, 2019, 10, 1127.	12.8	62
27	Atomic Resolution Defocused Electron Ptychography at Low Dose with a Fast, Direct Electron Detector. Scientific Reports, 2019, 9, 3919.	3.3	44
28	Formation and Healing of Defects in Atomically Thin GaSe and InSe. ACS Nano, 2019, 13, 5112-5123.	14.6	35
29	Molecular nitrogen promotes catalytic hydrodeoxygenation. Nature Catalysis, 2019, 2, 1078-1087.	34.4	63
30	Characterization of grain boundary disconnections in SrTiO3 Part II: the influence of superimposed disconnections on image analysis. Journal of Materials Science, 2019, 54, 3710-3725.	3.7	12
31	Atomic Resolution Transmission Electron Microscopy. Springer Handbooks, 2019, , 3-47.	0.6	4
32	Entrapped Single Tungstate Site in Zeolite for Cooperative Catalysis of Olefin Metathesis with BrÃ,nsted Acid Site. Journal of the American Chemical Society, 2018, 140, 6661-6667.	13.7	71
33	General synthesis and definitive structural identification of MN4C4 single-atom catalysts with tunable electrocatalytic activities. Nature Catalysis, 2018, 1, 63-72.	34.4	1,476
34	Hollow Electron Ptychographic Diffractive Imaging. Physical Review Letters, 2018, 121, 146101.	7.8	27
35	Low Dose Defocused Probe Electron Ptychography Using a Fast Direct Electron Detector. Microscopy and Microanalysis, 2018, 24, 186-187.	0.4	5
36	Fast and Low-dose Electron Ptychography. Microscopy and Microanalysis, 2018, 24, 224-225.	0.4	3

#	Article	IF	CITATIONS
37	Ultralong 1D Vacancy Channels for Rapid Atomic Migration during 2D Void Formation in Monolayer MoS ₂ . ACS Nano, 2018, 12, 7721-7730.	14.6	54
38	Imaging Structure and Magnetisation in New Ways Using 4D STEM. Microscopy and Microanalysis, 2018, 24, 180-181.	0.4	1
39	Atomic Structure and Dynamics of Single Platinum Atom Interactions with Monolayer MoS ₂ . ACS Nano, 2017, 11, 3392-3403.	14.6	126
40	Atomic structure and formation mechanism of sub-nanometer pores in 2D monolayer MoS ₂ . Nanoscale, 2017, 9, 6417-6426.	5.6	54
41	Characterisation of the Medipix3 detector for 60 and 80 keV electrons. Ultramicroscopy, 2017, 182, 44-53.	1.9	77
42	Snapshot 3D Electron Imaging of Structural Dynamics. Scientific Reports, 2017, 7, 10839.	3.3	10
43	Electron ptychographic microscopy for three-dimensional imaging. Nature Communications, 2017, 8, 163.	12.8	89
44	Electron Ptychographic Diffractive Imaging of Boron Atoms in LaB6 Crystals. Scientific Reports, 2017, 7, 2857.	3.3	37
45	Electron Ptychography: From 2D to 3D Reconstructions. Microscopy and Microanalysis, 2017, 23, 346-347.	0.4	0
46	Atomically Flat Zigzag Edges in Monolayer MoS ₂ by Thermal Annealing. Nano Letters, 2017, 17, 5502-5507.	9.1	70
47	Aberration measurement of the probe-forming system of an electron microscope using two-dimensional materials. Ultramicroscopy, 2017, 182, 195-204.	1.9	5
48	Phase Retrieval Quantitative Comparison Between Tilt-series Imaging in TEM and Position-resolved Coherent Diffractive Imaging in STEM. Microscopy and Microanalysis, 2017, 23, 470-471.	0.4	0
49	Using Advanced STEM Techniques to Unravel Key Issues in the Development of Next-Generation Nanostructures for Energy Storage. Microscopy and Microanalysis, 2017, 23, 1698-1699.	0.4	Ο
50	Dose-dependent high-resolution electron ptychography. Journal of Applied Physics, 2016, 119, .	2.5	9
51	One-Pot Synthesis of Lithium-Rich Cathode Material with Hierarchical Morphology. Nano Letters, 2016, 16, 7503-7508.	9.1	42
52	Atomic Structure and Spectroscopy of Single Metal (Cr, V) Substitutional Dopants in Monolayer MoS ₂ . ACS Nano, 2016, 10, 10227-10236.	14.6	96
53	Temperature dependence of atomic vibrations in mono-layer graphene. Journal of Applied Physics, 2015, 118, .	2.5	18
54	Controlled formation of closed-edge nanopores in graphene. Nanoscale, 2015, 7, 11602-11610.	5.6	38

Angus I Kirkland

#	Article	IF	CITATIONS
55	Temperature Dependence of the Reconstruction of Zigzag Edges in Graphene. ACS Nano, 2015, 9, 4786-4795.	14.6	68
56	Atomic Structure of Graphene Subnanometer Pores. ACS Nano, 2015, 9, 11599-11607.	14.6	75
57	Thermally Induced Dynamics of Dislocations in Graphene at Atomic Resolution. ACS Nano, 2015, 9, 10066-10075.	14.6	36
58	Partial Dislocations in Graphene and Their Atomic Level Migration Dynamics. Nano Letters, 2015, 15, 5950-5955.	9.1	37
59	Deterministic electron ptychography at atomic resolution. Physical Review B, 2014, 89, .	3.2	46
60	Inflating Graphene with Atomic Scale Blisters. Nano Letters, 2014, 14, 908-914.	9.1	37
61	The Role of the Bridging Atom in Stabilizing Odd Numbered Graphene Vacancies. Nano Letters, 2014, 14, 3972-3980.	9.1	44
62	Stability and Dynamics of the Tetravacancy in Graphene. Nano Letters, 2014, 14, 1634-1642.	9.1	68
63	The development of a 200kV monochromated field emission electron source. Ultramicroscopy, 2014, 140, 37-43.	1.9	46
64	Atomic Structure and Dynamics of Metal Dopant Pairs in Graphene. Nano Letters, 2014, 14, 3766-3772.	9.1	219
65	Influence of Shell Thickness and Surface Passivation on PbS/CdS Core/Shell Colloidal Quantum Dot Solar Cells. Chemistry of Materials, 2014, 26, 4004-4013.	6.7	129
66	Exit wave reconstruction of radiation-sensitive materials from low-dose data. Journal of Physics: Conference Series, 2014, 522, 012052.	0.4	4
67	Recording low and high spatial frequencies in exit wave reconstructions. Ultramicroscopy, 2013, 133, 26-34.	1.9	14
68	Assessing the precision of strain measurements using electron backscatter diffraction – part 1: Detector assessment. Ultramicroscopy, 2013, 135, 126-135.	1.9	43
69	Bond Length and Charge Density Variations within Extended Arm Chair Defects in Graphene. ACS Nano, 2013, 7, 9860-9866.	14.6	38
70	Gold–Palladium Core–Shell Nanocrystals with Size and Shape Control Optimized for Catalytic Performance. Angewandte Chemie - International Edition, 2013, 52, 1477-1480.	13.8	104
71	Assessing the precision of strain measurements using electron backscatter diffraction – Part 2: Experimental demonstration. Ultramicroscopy, 2013, 135, 136-141.	1.9	27
72	Dynamics of Single Fe Atoms in Graphene Vacancies. Nano Letters, 2013, 13, 1468-1475.	9.1	228

#	Article	IF	CITATIONS
73	Impurity induced non-bulk stacking in chemically exfoliated h-BN nanosheets. Nanoscale, 2013, 5, 2290.	5.6	20
74	Structural Reconstruction of the Graphene Monovacancy. ACS Nano, 2013, 7, 4495-4502.	14.6	131
75	A Study of Commercial Nanoparticulate γâ€Al ₂ O ₃ Catalyst Supports. ChemCatChem, 2013, 5, 2695-2706.	3.7	50
76	Toward 3D structural information from quantitative electron exit wave analysis. Journal of Physics: Conference Series, 2012, 371, 012057.	0.4	1
77	Exit wave reconstruction from focal series of HRTEM images, single crystal XRD and total energy studies on Sb _{<i>x</i>} WO _{3+<i>y</i>} (<i>x</i> â^¼ 0.11). Zeitschrift Fur Kristallographie - Crystalline Materials, 2012, 227, 341-349.	0.8	8
78	Toward electron exit wave tomography of amorphous materials at atomic resolution. Journal of Alloys and Compounds, 2012, 536, S94-S98.	5.5	2
79	Spatial control of defect creation in graphene at the nanoscale. Nature Communications, 2012, 3, 1144.	12.8	305
80	Atomic Structure of ABC Rhombohedral Stacked Trilayer Graphene. ACS Nano, 2012, 6, 5680-5686.	14.6	59
81	High Resolution ExitWave Restoration. Nanostructure Science and Technology, 2012, , 41-72.	0.1	3
82	Dislocation-Driven Deformations in Graphene. Science, 2012, 337, 209-212.	12.6	332
83	Controlled Radiation Damage and Edge Structures in Boron Nitride Membranes. ACS Nano, 2011, 5, 3977-3986.	14.6	33
84	Imaging the Active Surfaces of Cerium Dioxide Nanoparticles. ChemPhysChem, 2011, 12, 2397-2399.	2.1	20
85	Inside Cover: Imaging the Active Surfaces of Cerium Dioxide Nanoparticles (ChemPhysChem 13/2011). ChemPhysChem, 2011, 12, 2358-2358.	2.1	0
86	Resolving strain in carbon nanotubes at the atomic level. Nature Materials, 2011, 10, 958-962.	27.5	61
87	Finding phase information in the darkness. Journal of Physics: Conference Series, 2010, 241, 012013.	0.4	1
88	Exceeding Conventional Resolution Limits in High-Resolution Transmission Electron Microscopy Using Tilted Illumination and Exit-Wave Restoration. Microscopy and Microanalysis, 2010, 16, 409-415.	0.4	7
89	Transformations of gold nanoparticles investigated using variable temperature high-resolution transmission electron microscopy. Ultramicroscopy, 2010, 110, 506-516.	1.9	57
90	Aberration measurement using the Ronchigram contrast transfer function. Ultramicroscopy, 2010, 110, 891-898.	1.9	42

#	Article	IF	CITATIONS
91	Nanoscale Energy-Filtered Scanning Confocal Electron Microscopy Using a Double-Aberration-Corrected Transmission Electron Microscope. Physical Review Letters, 2010, 104, 200801.	7.8	46
92	Structural characterization of interfaces in epitaxial Fe/MgO/Fe magnetic tunnel junctions by transmission electron microscopy. Physical Review B, 2010, 82, .	3.2	22
93	Nanogold: A Quantitative Phase Map. ACS Nano, 2009, 3, 1431-1436.	14.6	238
94	Synthesis and Structural Characterization of Branched Palladium Nanostructures. Advanced Materials, 2009, 21, 2288-2293.	21.0	124
95	Atomic Imaging of Phase Transitions and Morphology Transformations in Nanocrystals. Advanced Materials, 2009, 21, 4992-4995.	21.0	104
96	Effect of amorphous layers on the interpretation of restored exit waves. Ultramicroscopy, 2009, 109, 237-246.	1.9	16
97	Atomic Structure Imaging Beyond Conventional Resolution Limits in the Transmission Electron Microscope. Physical Review Letters, 2009, 103, 126101.	7.8	26
98	Optimal tilt magnitude determination for aberration-corrected super resolution exit wave function reconstruction. Philosophical Transactions Series A, Mathematical, Physical, and Engineering Sciences, 2009, 367, 3755-3771.	3.4	17
99	Three-dimensional imaging in double aberration-corrected scanning confocal electron microscopy, Part II: Inelastic scattering. Ultramicroscopy, 2008, 108, 1567-1578.	1.9	47
100	DFT calculations of KI crystals formed within single-walled carbon nanotubes. Chemical Physics Letters, 2008, 466, 76-78.	2.6	6
101	Transmission electron microscopy without aberrations: Applications to materials science. Current Applied Physics, 2008, 8, 425-428.	2.4	11
102	Three-dimensional imaging in double aberration-corrected scanning confocal electron microscopy, Part I:. Ultramicroscopy, 2008, 108, 1558-1566.	1.9	60
103	Low-dose aberration corrected cryo-electron microscopy of organic specimens. Ultramicroscopy, 2008, 108, 1636-1644.	1.9	46
104	Combining Theory and Experiment in Determining the Surface Chemistry of Nanocrystals. Chemistry of Materials, 2008, 20, 5460-5463.	6.7	30
105	Direct Imaging of the Structure, Relaxation, and Sterically Constrained Motion of Encapsulated Tungsten Polyoxometalate Lindqvist Ions within Carbon Nanotubes. ACS Nano, 2008, 2, 966-976.	14.6	50
106	High-Resolution TEM and the Application of Direct and Indirect Aberration Correction. Microscopy and Microanalysis, 2008, 14, 60-67.	0.4	15
107	Aberration corrected TEM: current status and future prospects. Journal of Physics: Conference Series, 2008, 126, 012034.	0.4	3
108	Aberration corrected tilt series restoration. Journal of Physics: Conference Series, 2008, 126, 012042.	0.4	0

#	Article	IF	CITATIONS
109	Band-Gap Modification Induced in HgTe by Dimensional Constraint in Carbon Nanotubes: Effect of Nanotube Diameter on Microstructure. Springer Proceedings in Physics, 2008, , 213-216.	0.2	1
110	Electron nanodiffraction using sharply focused parallel probes. Applied Physics Letters, 2007, 90, 151104.	3.3	28
111	Atomic Resolution Transmission Electron Microscopy. , 2007, , 3-64.		2
112	Aberration-Corrected Imaging of Active Sites on Industrial Catalyst Nanoparticles. Angewandte Chemie - International Edition, 2007, 46, 3683-3685.	13.8	117
113	Atomic-Scale Detection of Organic Molecules Coupled to Single-Walled Carbon Nanotubes. Journal of the American Chemical Society, 2007, 129, 10966-10967.	13.7	63
114	Ultrahigh resolution imaging of local structural distortions in intergrowth tungsten bronzes. Ultramicroscopy, 2007, 107, 501-506.	1.9	8
115	Correlation of Structural and Electronic Properties in a New Low-Dimensional Form of Mercury Telluride. Physical Review Letters, 2006, 96, 215501.	7.8	78
116	Confocal operation of a transmission electron microscope with two aberration correctors. Applied Physics Letters, 2006, 89, 124105.	3.3	92
117	Crystallization of 2H and 4H PbI2in Carbon Nanotubes of Varying Diameters and Morphologies. Chemistry of Materials, 2006, 18, 2059-2069.	6.7	86
118	Comparisons of Linear and Nonlinear Image Restoration. Microscopy and Microanalysis, 2006, 12, 469-475.	0.4	15
119	Local Measurement and Computational Refinement of Aberrations for HRTEM. Microscopy and Microanalysis, 2006, 12, 461-468.	0.4	24
120	The application of spherical aberration correction and focal series restoration to high-resolution images of platinum nanocatalyst particles. Journal of Physics: Conference Series, 2006, 26, 25-28.	0.4	3
121	Structural correlation of band-gap modifications induced in mercury telluride by dimensional constraint in single walled carbon nanotubes. Physica Status Solidi (B): Basic Research, 2006, 243, 3257-3262.	1.5	14
122	On the importance of fifth-order spherical aberration for a fully corrected electron microscope. Ultramicroscopy, 2006, 106, 301-306.	1.9	57
123	HREM of the {111} surfaces of iron oxide nanoparticles. Micron, 2006, 37, 389-395.	2.2	9
124	HREM of metallized {111} iron oxide nanoparticle surfaces. Journal of Physics: Conference Series, 2006, 26, 191-194.	0.4	2
125	Materials Advances through Aberration-Corrected Electron Microscopy. MRS Bulletin, 2006, 31, 36-43.	3.5	89
126	Observation of octahedral cation coordination on the {111} surfaces of iron oxide nanoparticles. Applied Physics Letters, 2006, 88, 093124.	3.3	18

Angus I Kirkland

#	Article	IF	CITATIONS
127	Structure Determination of Atomically Controlled Crystal Architectures Grown within Single Wall Carbon Nanotubes. Microscopy and Microanalysis, 2005, 11, 401-409.	0.4	23
128	Lal ₂ @(18,3)SWNT: The Unprecedented Structure of a Lal ₂ "Crystal,― Encapsulated within a Single-Walled Carbon Nanotube. Microscopy and Microanalysis, 2005, 11, 421-430.	0.4	10
129	A versatile double aberration-corrected, energy filtered HREM/STEM for materials science. Ultramicroscopy, 2005, 103, 7-15.	1.9	89
130	Calculations of HREM image intensity using Monte Carlo integration. Ultramicroscopy, 2005, 104, 271-280.	1.9	14
131	Experimental evaluation of a spherical aberration-corrected TEM and STEM. Microscopy (Oxford,) Tj ETQq1 1 0.7	84314 rgE 1.5	3T /Qverlock
132	Aberration-corrected HREM/STEM for semiconductor research., 2005,, 177-182.		1
133	A new method for the determination of the wave aberration function for high-resolution TEM Ultramicroscopy, 2004, 99, 115-123.	1.9	63
134	Resolution extension and exit wave reconstruction in complex HREM. Ultramicroscopy, 2004, 98, 99-114.	1.9	72
135	"Indirect―High-Resolution Transmission Electron Microscopy: Aberration Measurement and Wavefunction Reconstruction. Microscopy and Microanalysis, 2004, 10, 401-413.	0.4	71
136	Imaging and Characterization of Molecules and One-Dimensional Crystals Formed within Carbon Nanotubes. MRS Bulletin, 2004, 29, 265-271.	3.5	21
137	Structural investigation of MoS2core–shell nanoparticles formed by an arc discharge in water. Nanotechnology, 2003, 14, 913-917.	2.6	36
138	A composite method for the determination of the chirality of single walled carbon nanotubes. Journal of Microscopy, 2003, 212, 152-157.	1.8	39
139	Structural characterization of the n = 5 layered perovskite neodymium titanate using high-resolution transmission electron microscopy and image reconstruction. Acta Crystallographica Section B: Structural Science, 2003, 59, 449-455.	1.8	5
140	An encapsulated helical one-dimensional cobalt iodide nanostructure. Nature Materials, 2003, 2, 788-791.	27.5	156
141	Calculations of spherical aberration-corrected imaging behaviour. Journal of Electron Microscopy, 2003, 52, 359-364.	0.9	18
142	Integral atomic layer architectures of 1D crystals inserted into single walled carbon nanotubes. Chemical Communications, 2002, , 1319-1332.	4.1	208
143	Structural Characterization of Atomically Regulated Nanocrystals Formed within Single-Walled Carbon Nanotubes Using Electron Microscopy. Accounts of Chemical Research, 2002, 35, 1054-1062.	15.6	103
144	Cation segregation in Nb16W18O94 using high angle annular dark field scanning transmission electron microscopy and image processing. Journal of Microscopy, 2002, 206, 1-6.	1.8	21

#	Article	IF	CITATIONS
145	A new method for the determination of the wave aberration function for high resolution TEM. Ultramicroscopy, 2002, 92, 89-109.	1.9	131
146	Structural changes induced in nanocrystals of binary compounds confined within single walled carbon nanotubes: a brief review. Inorganica Chimica Acta, 2002, 330, 1-12.	2.4	85
147	Direct and Indirect Electron Microscopy of Encapsulated Nanocrystals. Topics in Catalysis, 2002, 21, 139-154.	2.8	6
148	The characterization of sub-nanometer scale structures within single walled carbon nanotubes. AIP Conference Proceedings, 2001, , .	0.4	5
149	The Crystallography of Metal Halides formed within Single Walled Carbon Nanotubes. Materials Research Society Symposia Proceedings, 2000, 633, 14311.	0.1	2
150	Characterisation of the signal and noise transfer of CCD cameras for electron detection. Microscopy Research and Technique, 2000, 49, 269-280.	2.2	110
151	Discrete Atom Imaging of One-Dimensional Crystals Formed Within Single-Walled Carbon Nanotubes. Science, 2000, 289, 1324-1326.	12.6	407
152	The effects of electron and photon scattering on signal and noise transfer properties of scintillators in CCD cameras used for electron detection. Ultramicroscopy, 1998, 75, 23-33.	1.9	87
153	Multiple beam tilt microscopy for super resolved imaging. Journal of Electron Microscopy, 1997, 46, 11-22.	0.9	51
154	A Joint Structural Characterization of Colloidal Platinum by EXAFS and High-Resolution Electron Microscopy. Angewandte Chemie International Edition in English, 1989, 28, 590-593.	4.4	41
155	Structure and growth of colloidal metal particles. Journal of Chemical Physics, 1989, 91, 603-611.	3.0	27
156	A Morphology-Selective Copper Organosol. Angewandte Chemie International Edition in English, 1988, 27, 1530-1533.	4.4	84
157	The Morphology and Microstructure of Colloidal Silver and Gold. Angewandte Chemie International Edition in English, 1987, 26, 676-678.	4.4	58